Bifurcation of surface pattern in epitaxial thin films under anisotropic stresses

Yaoyu Pang and Rui Huang[a)]
Department of Aerospace Engineering and Engineering Mechanics, University of Texas, Austin, Texas 78712

(Received 12 October 2006; accepted 16 November 2006; published online 23 January 2007)

Surface instability of epitaxial thin films leads to a variety of surface patterns. Anisotropy in surface and bulk properties has profound effects on the dynamics of pattern formation. In this paper, we theoretically predict that under anisotropic mismatch stresses, a bifurcation of surface pattern occurs in addition to generic symmetry breaking from isotropic systems. Numerical simulations based on a nonlinear evolution equation demonstrate pattern selection at an early stage and nontrivial patterns for long-time evolution. © *2007 American Institute of Physics*. [DOI: 10.1063/1.2430771]

I. INTRODUCTION

Stress plays an important role in pattern formation at solid surfaces. A macroscopically planar surface of a stressed solid is thermodynamically unstable, driven by competition between elastic strain energy and surface energy.[1] Experimental investigations have observed deep grooving and cracklike surface patterns in a number of systems,[2] which have been theoretically understood as a result of nonlinear stress effect.[3–5] Recently, Berger *et al.*[6] analyzed the morphological instability of biaxially stressed solids during a melting-crystallization process and predicted nontrivial dynamics of pattern formation when the two principal stresses at the solid surface take opposite signs (i.e., tension and compression). Numerical simulations by Paret[7] confirmed the analytical prediction and showed intricate patterns in the nonlinear regime.

The stress-driven surface instability in epitaxial systems has been studied extensively as a route to produce self-assembled surface structures.[8] An epitaxial thin film is stressed due to lattice mismatch with underlying substrate. Interaction between film and substrate further complicates the dynamics of surface evolution, leading to a large variety of surface patterns, such as self-assembled quantum dots. Previous studies have shown that the shape of an individual dot is largely controlled by anisotropy in surface energy,[9] while the spatial organization of dots is strongly influenced by long-range interactions through elastic stress fields.[10] Experimental investigations have explored various techniques to manipulate the stress field in order to achieve directed organization of quantum dots.[11] Theoretically, although a few recent works considered the effect of elastic anisotropy,[12] systematic studies on the dynamics of pattern formation under the influence of anisotropic and/or nonuniform stresses are lacking.

Recently, we developed an evolution equation for epitaxial thin films that takes into account nonlinear effects of stress and wetting interaction at the film/substrate interface.[5] This enables us to theoretically study the dynamics of long-time evolution over a large surface area. Under an equibiaxial mismatch stress, the system is isotropic (material anisotropy is ignored), and numerical simulations predict self-assembly of circular islands. Introducing any anisotropy would break the symmetry. In this paper, we show that, in addition to the generic symmetry breaking, a bifurcation in pattern selection occurs when the film is subjected to an anisotropic mismatch stress. While similar bifurcation was predicted for biaxially stressed solids,[6,7] the epitaxial system exhibits even richer dynamics in forming elongated islands or tilted line patterns. Practically, anisotropic mismatch stresses can be obtained in many systems with either an elastically anisotropic film or an anisotropic substrate. Examples include Ge on Si (113)[13] and hexagonally structured $ErSi_2$ on Si (001).[14]

II. EVOLUTION EQUATION

At the reference state, the system consists of a uniformly stressed epitaxial film of thickness h_0 on a substrate. We set up the Cartesian coordinates coinciding with the principal directions of the mismatch stress. The two principal stresses in the plane of the film are $\sigma_{11}^{(0)}=\sigma_1$ and $\sigma_{22}^{(0)}=\sigma_2$; other stress components are zero. Upon annealing, the film surface evolves, with an instantaneous thickness profile, $h(x_1,x_2,t)$, where t is the time of evolution. Assuming surface diffusion as the dominant process of mass transport and a linear kinetic law, we obtain an evolution equation for the thickness profile[5]

$$\frac{\partial h}{\partial t}=\Omega^2 M\frac{\partial^2}{\partial x_\alpha \partial x_\alpha}[(U_E-\gamma\kappa+U_W)\sqrt{1+h_\beta h_\beta}], \tag{1}$$

where U_E is the elastic strain energy density at the surface, U_W the wetting potential, γ the surface energy density, κ the surface curvature, M the surface mobility, Ω the atomic volume, and $h_\alpha=\partial h/\partial x_\alpha$ the surface gradient. A repeated Greek subscript implies summation over 1 and 2.

Although both the film and the substrate are considered linear elastic, the boundary condition at the evolving surface renders a nonlinear boundary-value problem, typically requiring significant effort to determine the strain energy U_E

[a)]Electronic mail: ruihuang@mail.utexas.edu

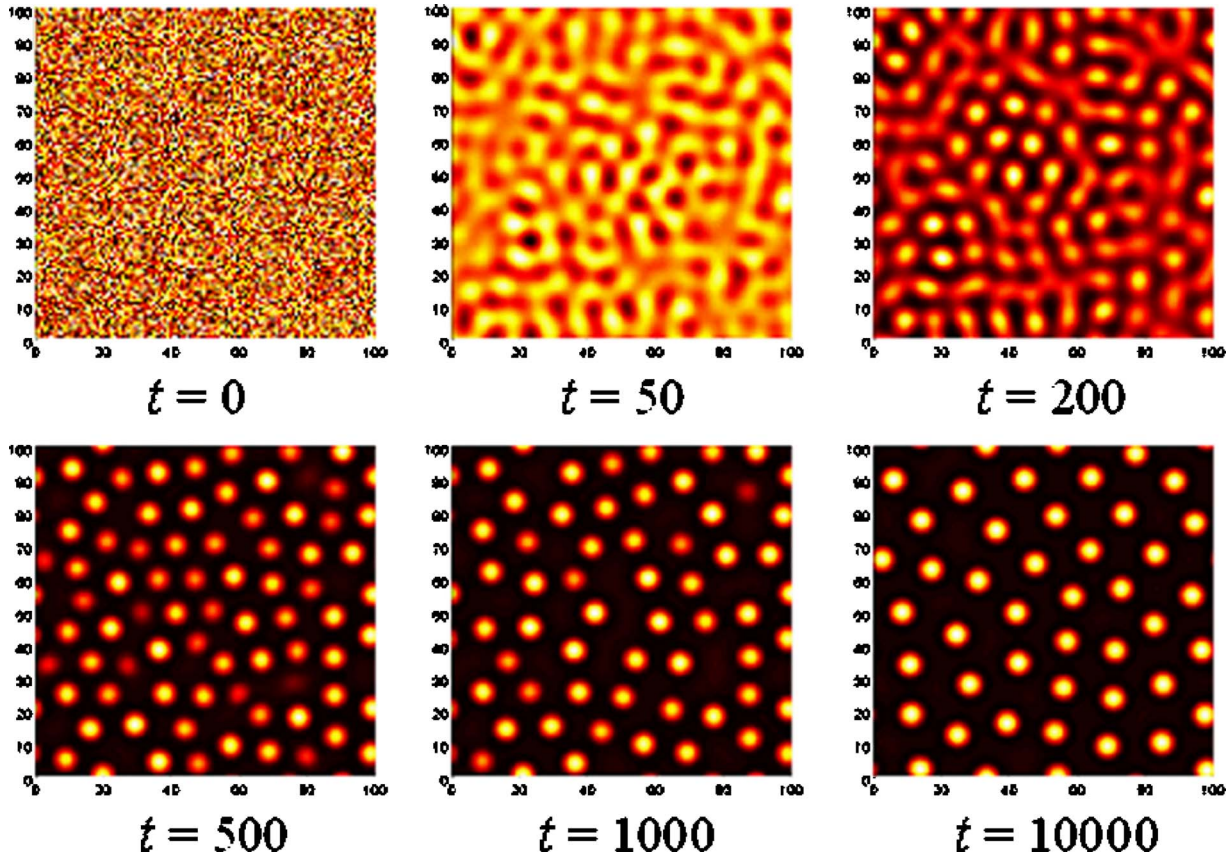

FIG. 1. (Color online) Contours of simulated surface morphology, $h(x_1,x_2,t)$, under an equibiaxial stress ($c=1$). Evolution starts from a random initial perturbation at $t=0$. A bright spot represents a crest.

during evolution.[9,12] Previously, we solved the boundary-value problem via an asymptotic approach,[5] which leads to a series expansion of the strain energy

$$U_E = U_E^{(0)} + U_E^{(1)} + U_E^{(2)} + \cdots, \tag{2}$$

where, for the present system,

$$U_E^{(0)} = \frac{1}{2E_f}(\sigma_1^2 + \sigma_2^2 - 2\nu_f\sigma_1\sigma_2), \tag{3}$$

$$U_E^{(1)} = \sigma_1\frac{\partial u_1^{(1)}}{\partial x_1} + \sigma_2\frac{\partial u_2^{(1)}}{\partial x_2}, \tag{4}$$

$$U_E^{(2)} = \frac{1+\nu_f}{E_f}\sigma_{\alpha\beta}^{(0)}\sigma_{\alpha\gamma}^{(0)}h_\beta h_\gamma + \sigma_{\alpha\beta}^{(0)}\frac{\partial u_\alpha^{(2)}}{\partial x_\beta} + \frac{1}{2}\sigma_{\alpha\beta}^{(1)}\frac{\partial u_\alpha^{(1)}}{\partial x_\beta}. \tag{5}$$

The first term $U_E^{(0)}$ is a constant, corresponding to the strain energy density at the reference state as given in Eq. (3). To focus on the effect of stress anisotropy, the present study assumes an otherwise isotropic system, with E and ν as Young's modulus and Poisson's ratio, respectively, and subscripts f and s denoting film and substrate, both elastically isotropic.

The second term $U_E^{(1)}$ is to the first order of surface perturbation. In Eq. (4), the surface displacement $u_\alpha^{(1)}$ is related to the perturbed surface profile as the first-order solution to the boundary-value problem

$$\hat{u}_\alpha^{(1)} = ik_\gamma C_{\alpha\beta}\sigma_{\beta\gamma}^{(0)}\hat{h}, \tag{6}$$

where $\hat{}$ on top indicates two-dimensional Fourier transform of the quantity with respect to x_1 and x_2, k_γ is the component of wave vector with $k=\sqrt{k_1^2+k_2^2}$, and $C_{\alpha\beta}$ is from the compliance matrix

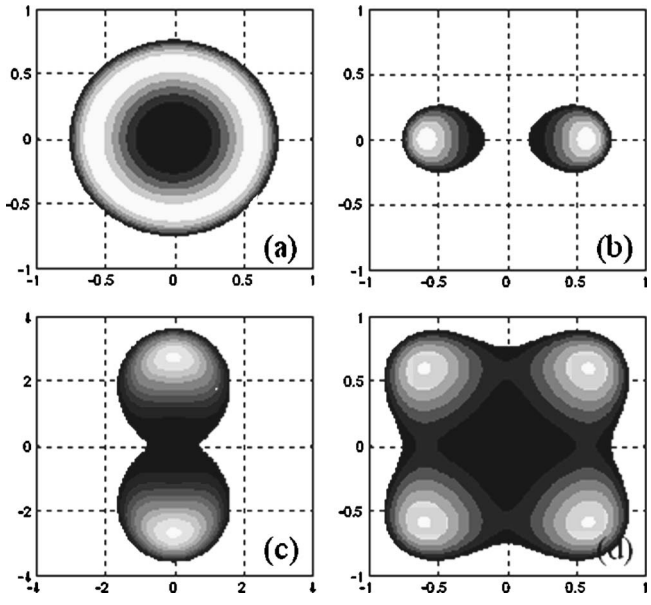

FIG. 2. Contours of the growth rate, $s(k_1,k_2)$, under various stress anisotropy: (a) $c=1$, (b) $c=0$, (c) $c=2$, and (d) $c=-1$.

$$\mathbf{C}=\frac{2(1+\nu_s)}{E_s k^3}\begin{bmatrix}(1-\nu_s)k^2+\nu_s k_2^2 & -\nu_s k_1 k_2 & -\frac{1-2\nu_s}{2}ik_1 k\\ -\nu_s k_1 k_2 & (1-\nu_s)k^2+\nu_s k_1^2 & -\frac{1-2\nu_s}{2}ik_2 k\\ \frac{1-2\nu_s}{2}ik_1 k & \frac{1-2\nu_s}{2}ik_2 k & (1-\nu_s)k^2\end{bmatrix}. \tag{7}$$

The third term at the right-hand side of Eq. (2) is to the second order of surface perturbation, which is the leading nonlinear term. The higher order terms are ignored. In Eq. (5), the first-order stress is related to the gradient of surface displacement by Hooke's law,

$$\sigma_{\alpha\beta}^{(1)}=\frac{E_f}{2(1+\nu_f)}\left(\frac{\partial u_\alpha^{(1)}}{\partial x_\beta}+\frac{\partial u_\beta^{(1)}}{\partial x_\alpha}+\frac{2\nu_f}{1-\nu_f}\frac{\partial u_\gamma^{(1)}}{\partial x_\gamma}\delta_{\alpha\beta}\right), \tag{8}$$

and the second-order displacement is given by

$$\hat{u}_\alpha^{(2)}=C_{\alpha\beta}\hat{\varphi}_\beta+C_{\alpha 3}\hat{\phi}, \tag{9}$$

where $\varphi_\beta=\sigma_{\beta\gamma}^{(1)}h_\gamma$ and $\phi=\sigma_{\alpha\beta}^{(0)}h_\alpha h_\beta$.

For the wetting potential in Eq. (1), we adopt the transition-layer model,[15] which assumes a transition of the surface energy density as

$$\gamma(h)=\frac{1}{2}(\gamma_f+\gamma_s)+\frac{1}{\pi}(\gamma_f-\gamma_s)\arctan\left(\frac{h}{b}\right), \tag{10}$$

where the length b characterizes the transition thickness between the film and the substrate. Equation (10) leads to a nonlinear wetting potential[15]

$$U_W=\frac{b(\gamma_f-\gamma_s)}{\pi(b^2+h^2)\sqrt{1+h_\alpha h_\alpha}}. \tag{11}$$

III. RESULTS AND DISCUSSIONS

The nonlinear evolution equation can be solved efficiently by a spectral method.[5] The numerical results are normalized by a length scale $L=\gamma_f E_s/[2(1-\nu_s^2)\sigma_1^2]$ and a time scale $\tau=L^4/(\Omega^2 M\gamma_f)$. The parameters used in simulations are $E_f/E_s=1.1$, $\gamma_s/\gamma_f=1.2$, $h_0=0.1L$, $b=0.001L$, and $\nu_f=\nu_s=0.25$. When the film is subjected to an equibiaxial mismatch stress ($\sigma_1=\sigma_2=\sigma_0$), the system is isotropic. As shown in Fig. 1, the surface first evolves into a chaotic pattern and

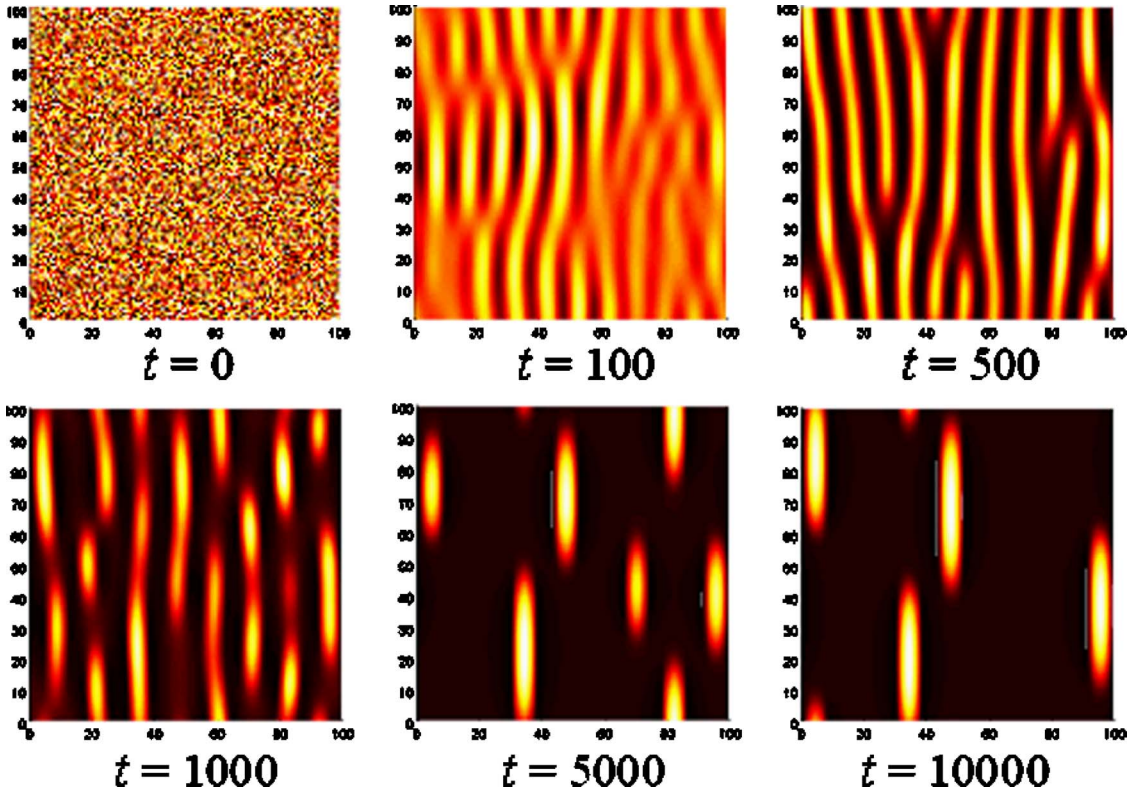

FIG. 3. (Color online) Contours of simulated surface morphology, $h(x_1,x_2,t)$, with $c=0$.

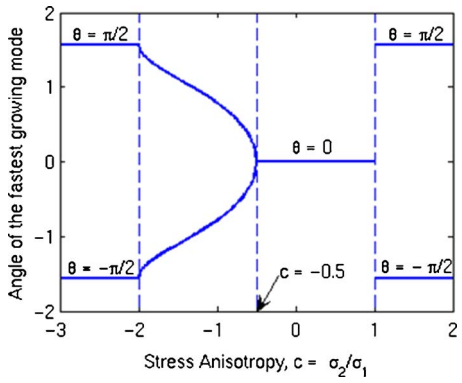

FIG. 4. Angle(s) of the fastest growing mode as a function of stress anisotropy (ν_s=0.25).

then breaks up into circular dots. Subsequently, the pattern undergoes a coarsening process with the number density of dots decreasing. After a long time, the pattern is stabilized, with a nearly uniform dot size and random organization. The rotational symmetry of the isotropic system is responsible for the initial chaotic pattern as well as the randomly organized circular dots. It should be noted that the shape transition of individual islands predicted by previous works[9] is not captured in the present simulation due to the assumption of isotropic surface energy. Here we focus on macroscopic shape and large-area organization of islands rather than detailed surface facets and steps at atomic scale.

The rotational symmetry is broken when the mismatch stress is anisotropic (i.e., $\sigma_1 \neq \sigma_2$), which can be shown analytically by a linear analysis. We define $c=\sigma_2/\sigma_1$ as the factor of stress anisotropy. Taking only the linear part of Eq. (1), we obtain

$$\frac{\partial \hat{h}}{\partial t} = s(k_1,k_2)\hat{h}, \tag{12}$$

where

$$s(k_1,k_2) = \frac{1}{k(1-\nu_s)}[(k_1^2+k_2^2c^2)k^2 - (k_1^2+ck_2^2)^2\nu_s] - k^4 + \frac{2bL^2(\gamma_f-\gamma_s)}{\pi h_0^3\gamma_f}k^2. \tag{13}$$

Therefore, in the linear regime, each Fourier component of the surface profile grows (or decays) exponentially, with the growth rate s as a function of the wave vector (k_1,k_2). When $c=1$, the contour plots of the growth rate are concentric circles [Fig. 2(a)], indicating rotational symmetry in the isotropic system. The growth rate is positive in an annular region, and the fastest growing mode corresponds to a circle. The symmetry is broken when $c\neq 1$. As shown in Figs. 2(b) and 2(c), the fastest growing mode corresponds to two points (white spots) located on one of the principal axes. This suggests that the initial evolution would develop parallel line patterns perpendicular to the principal direction. This is confirmed by numerical simulation as shown in Fig. 3 for $c=0$. A parallel line pattern emerges at the early stage of evolution. The nonlinear effects of stress and wetting take over for

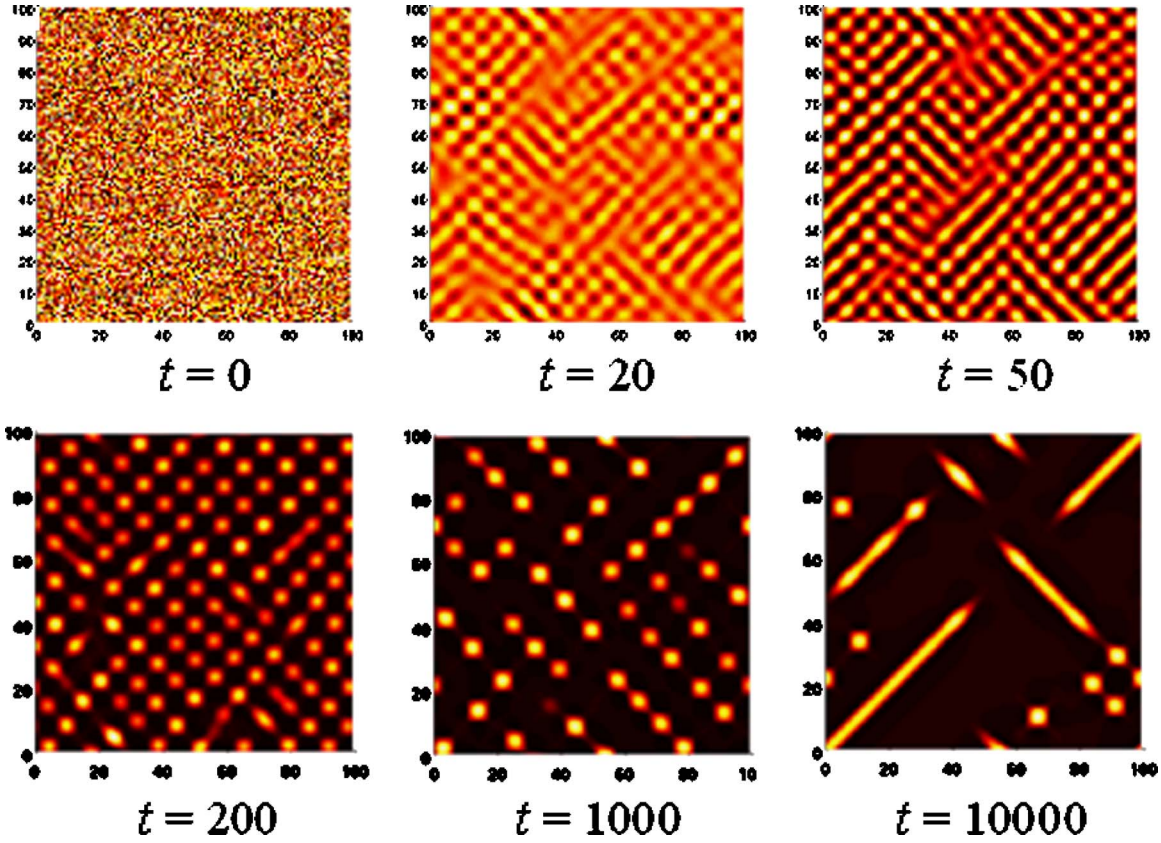

FIG. 5. (Color online) Contours of simulated surface morphology, $h(x_1,x_2,t)$, with $c=-1$.

long-time evolution, breaking up the lines into elongated islands.

The generic symmetry breaking persists when c becomes negative, with the principal mismatch stresses tensile in one direction and compressive in the orthogonal direction. In addition, a bifurcation occurs at a critical value. As shown in Fig. 2(d) for $c=-1$, the fastest growing mode now corresponds to four points located at angles $\pm 45°$ from the principal directions; i.e., the two white spots in Fig. 2(b) have split into four. We define the angle θ of wave vector such that $k_1=k\cos\theta$ and $k_2=k\sin\theta$ in Eq. (13). Setting $\partial s/\partial\theta=0$ leads to

$$(c-1)[(1-\nu_s)(1+c)-\nu_s(1-c)\cos 2\theta]\sin\theta\cos\theta=0. \tag{14}$$

When $c=1$, $\partial s/\partial\theta=0$ all around, thus no particular angle is selected for the fastest growth. When $c\neq 1$, the angle of the fastest growing mode can be determined by examining the second derivative of the growth rate. For $0.5>\nu_s>0$, three cases exist: (I) When $1>c>-(1-2\nu_s)$, $\sin\theta=0$ for the fastest growth, giving $\theta=0$. (II) When $c>1$ or $c<-(1-2\nu_s)^{-1}$, the fastest growing mode corresponds to $\cos\theta=0$, and thus $\theta=\pm 90°$. Cases I and II are equivalent upon switching σ_1 and σ_2. (III) When $-(1-2\nu_s)^{-1}<c<-(1-2\nu_s)$, the angle of the fastest growing mode is given by

$$\cos 2\theta=\frac{(1+c)(1-\nu_s)}{(1-c)\nu_s}. \tag{15}$$

Figure 4 plots the angle of the fastest growing mode as a function of stress anisotropy. A pitchfork bifurcation occurs at $c=-(1-2\nu_s)^{\pm 1}$. In between, the angle rotates from one principal direction to another, through two equivalent paths (clockwise or counterclockwise). In the present system, there exist two types of transition: a step transition at $c=1$ as the result of generic symmetry breaking and a smooth transition from $c=-(1-2\nu_s)$ to $c=-(1-2\nu_s)^{-1}$ via the bifurcation. Similar bifurcation patterns were reported for binary compositional fields in self-assembled monolayers.[16]

Figure 5 shows a simulated evolution sequence of surface pattern with $c=-1$. At the early stage, as opposed to the parallel line pattern in Fig. 3, the two angles of the fastest growth, $\theta=\pm 45°$, compete, leading to a diamond pattern. Subsequently, square-shaped islands form and undergo coarsening. Interestingly, after a long time, the islands coalesce to form tilted lines. The competition of the two tilting directions ($\pm 45°$) leads to the coexistence of long and short (broken) lines. Compared to previous studies on stressed solids,[6,7] the long-time dynamics of pattern evolution in the epitaxial system is more complicated due to film-substrate interaction.

IV. CONCLUDING REMARKS

The present study considers the effect of stress anisotropy in an otherwise isotropic epitaxial system. In real systems, stress anisotropy is usually coupled with other material anisotropy. For example, in an epitaxial system with Ge on Si (113), the two principal directions of the mismatch stress are 38° clockwise (σ_1) and 52° counterclockwise (σ_2) from Si[$33\bar{2}$], and the ratio $c=0.76$. Considering only the stress anisotropy would predict elongated Ge islands in the direction perpendicular to σ_1, i.e., 52° counterclockwise from Si[$33\bar{2}$]. However, in experiments, Ge lines parallel to Si[$33\bar{2}$] were observed.[13] This discrepancy may be resolved by including effects of elastic anisotropy and surface energy anisotropy. The interactions among different anisotropy would further complicate and also enrich the dynamics of pattern formation in the epitaxial system, which will be left for future studies.

ACKNOWLEDGMENT

This work is supported by the Department of Energy through Grant No. DE-FG02-05ER46230.

[1] R. J. Asaro and W. A. Tiller, Metall. Trans. **3**, 1789 (1972); M. A. Grinfeld, Sov. Phys. Dokl. **31**, 831 (1986); D. J. Srolovitz, Acta Metall. **37**, 621 (1989).
[2] R. H. Torii and S. Balibar, J. Low Temp. Phys. **89**, 391 (1992); J. Berrehar, C. Caroli, C. Lapersonne-Meyer, and M. Schott, Phys. Rev. B **46**, 13487 (1993).
[3] W. H. Yang and D. J. Srolovitz, Phys. Rev. Lett. **71**, 1593 (1993); J. Mech. Phys. Solids **42**, 1551 (1994).
[4] B. J. Spencer and D. I. Meiron, Acta Metall. Mater. **42**, 3629 (1994); Y. Xiang and E. Weinan, J. Appl. Phys. **91**, 9414 (2002).
[5] Y. Pang and R. Huang, Phys. Rev. B **74**, 075413 (2006).
[6] P. Berger, P. Kohlert, K. Kassner, C. Misbah, Phys. Rev. Lett. **90**, 176103 (2003).
[7] J. Paret, Phys. Rev. E **72**, 011105 (2005).
[8] D. E. Jesson, S. J. Pennycook, J.-M. Baribeau, and D. C. Houghton, Phys. Rev. Lett. **71**, 1744 (1993); R. Notzel, J. Temmyo, and T. Tamamura, Nature (London) **369**, 131 (1994); C. S. Ozkan, W. D. Nix, and H. Gao, Appl. Phys. Lett. **70**, 2247 (1997); J. L. Gray, R. Hull, and J. A. Floro, *ibid.* **81**, 2445 (2002); T. Mano, R. Nötzel, G. J. Hamhuis, T. J. Eijkemans, and J. H. Wolter, J. Appl. Phys. **92**, 4043 (2002); D. Granados and J. M. Garcia, Appl. Phys. Lett. **82**, 2401 (2003); K. Alchalabi, D. Zimm, G. Kostorz, and H. Zogg, Phys. Rev. Lett. **90**, 026104 (2003).
[9] C.-H. Chiu, Appl. Phys. Lett. **75**, 3473 (1999); Y. W. Zhang, Phys. Rev. B **61**, 10388 (2000); Y. W. Zhang and A. F. Bower, Appl. Phys. Lett. **78**, 2706 (2001); T. V. Savina, A. A. Golovin, S. H. Davis, A. A. Nepomnyashchu, and P. W. Voorhees, Phys. Rev. E **67**, 021606 (2003).
[10] J. A. Floro, G. A. Lucadamo, E. Chason, L. B. Freund, M. Sinclair, R. D. Twesten, and R. Q. Hwang, Phys. Rev. Lett. **80**, 4717 (1998); J. A. Floro, M. B. Sinclair, E. Chason, L. B. Freund, R. D. Twesten, R. Q. Hwang, and G. A. Lucadamo, Phys. Rev. Lett. **84**, 701 (2000).
[11] Q. Xie, A. Madhukar, P. Chen, and N. P. Kobayashi, Phys. Rev. Lett. **75**, 2542 (1995); T. I. Kamins and R. S. Williams, Appl. Phys. Lett. **71**, 1201 (1997); G. Jin, J. L. Liu, S. G. Thomas, Y. H. Luo, K. L. Wang, and Bich-Yen Nguyen, *ibid.* **75**, 2752 (1999); T. Ogino, Y. Homma, Y. Kobayashi, H. Hibino, K. Prabhakaran, K. Sumitomo, H. Omi, S. Suzuki, T. Yamashita, D. J. Bottomley, F. Ling, and A. Kaneko, Surf. Sci. **514**, 1 (2002); B. Yang, F. Liu, and M. G. Lagally, Phys. Rev. Lett. **92**, 025502 (2004).
[12] S. P. A. Gill, Thin Solid Films **423**, 136 (2003); Y. Ni, L. H. He, and A. K. Soh, J. Cryst. Growth **284**, 281 (2005); Y. W. Zhang, Appl. Phys. Lett. **87**, 121916 (2005); P. Liu, Y. W. Zhang, and C. Lu, *ibid.* **88**, 041922 (2006).
[13] H. Omi and T. Ogino, Appl. Phys. Lett. **71**, 2163 (1997); Phys. Rev. B **59**, 7521 (1999).
[14] Y. Chen, D. A. A. Ohlberg, G. Medeiros-Ribeiro, Y. A. Chang, and R. S. Williams, Appl. Phys. A: Mater. Sci. Process. **75**, 353 (2002).
[15] B. J. Spencer, Phys. Rev. B **59**, 2011 (1999).
[16] W. Lu and Z. Suo, Phys. Rev. B **65**, 085401 (2002); R. V. Kukta, N. Vasiljevic, N. Dimitrov, and K. Sieradzki, Phys. Rev. Lett. **95**, 186103 (2005).